mathematics

MDPI

Article

Entropy Analysis of Sutterby Nanofluid Flow over a Riga Sheet with Gyrotactic Microorganisms and Cattaneo–Christov Double Diffusion

Muhammad Faizan [1], Farhan Ali [1], Karuppusamy Loganathan [2,3,*], Aurang Zaib [1], Ch Achi Reddy [4] and Sara I. Abdelsalam [5,6,*]

[1] Department of Mathematical Sciences, Federal Urdu University of Arts, Sciences & Technology, Karachi 75300, Pakistan
[2] Research and Development Wing, Live4Research, Tiruppur 638106, India
[3] Department of Mathematics and Statistics, Manipal University Jaipur, Jaipur-303007, India
[4] Department of Science and Humanities, MLR Institute of Technology, Hyderabad 500043, India
[5] Instituto de Ciencias Matemáticas (ICMAT) (CSIC-UAM-UCM-UC3M), 28049 Madrid, Spain
[6] Basic Science, Faculty of Engineering, The British University in Egypt, Al-Shorouk City, Cairo 11837, Egypt
* Correspondence: loganathankaruppusamy304@gmail.com (K.L.); sara.abdelsalam@bue.edu.eg (S.I.A.)

Abstract: In this article, a Riga plate is exhibited with an electric magnetization actuator consisting of permanent magnets and electrodes assembled alternatively. This exhibition produces electromagnetic hydrodynamic phenomena over a fluid flow. A new study model is formed with the Sutterby nanofluid flow through the Riga plate, which is crucial to the structure of several industrial and entering advancements, including thermal nuclear reactors, flow metres and nuclear reactor design. This article addresses the entropy analysis of Sutterby nanofluid flow over the Riga plate. The Cattaneo–Christov heat and mass flux were used to examine the behaviour of heat and mass relaxation time. The bioconvective motile microorganisms and nanoparticles are taken into consideration. The system of equations for the current flow problems is converted from a highly non-linear partial system to an ordinary system through an appropriate transformation. The effect of the obtained variables on velocity, temperature, concentration and motile microorganism distributions are elaborated through the plots in detail. Further, the velocity distribution is enhanced for a greater Deborah number value and it is reduced for a higher Reynolds number for the two cases of pseudoplastic and dilatant flows. Microorganism distribution decreases with the increased magnitude of Peclet number, Bioconvection Lewis number and microorganism concentration difference number. Two types of graphical outputs are presented for the Sutterby fluid parameter ($\beta = -2.5$, $\beta = 2.5$). Finally, the validation of the present model is achieved with the previously available literature.

Keywords: Sutterby nanofluid; Riga plate; entropy analysis; bioconvection; microorganisms; HAM

MSC: 76D05; 35Q79; 76A05

Citation: Faizan, M.; Ali, F.; Loganathan, K.; Zaib, A.; Reddy, C.A.; Abdelsalam, S.I. Entropy Analysis of Sutterby Nanofluid Flow over a Riga Sheet with Gyrotactic Microorganisms and Cattaneo–Christov Double Diffusion. *Mathematics* **2022**, *10*, 3157. https://doi.org/10.3390/math10173157

Academic Editors: Maria Luminița Scutaru, Catalin I. Pruncu, Vasily Novozhilov, Marco Pedroni and Xiangmin Jiao

Received: 12 July 2022
Accepted: 30 August 2022
Published: 2 September 2022

1. Introduction

The rate of heat transport characteristics has received increasing attention from various scientists owing to its tremendous industrial features, for example, in mechanical, optical, electrical and cooling instruments. The rate of heat transport increment is very crucial in depositing energy. Therefore, researchers have focused on the investigation of a new type of fluid that is a mixture of nanoparticles with a size of 100 nm and larger thermophysical properties than ordinary fluids, known as nanoliquids. A nanoliquid is a colloidal suspension of the nanoparticle's thermal behaviour in the ordinary fluid. The first attempt was conducted by Choi et al. [1] in 1995. They showed the thermal conductivity of nanoliquids by adding nanosized particles. Later, Buongiorno [2] used this understanding of nanofluid to achieve a mathematical form by adding Brownian and Thermophoretic

terms. A mixed convection nanofluid flow with different geometries was presented by Hussain et al. [3,4]. Haq et al. [5] studied the second law analysis on a cross nanofluid. The MHD mixed convective flow of CNTs/Al_2O_3 nanofluid in water past a heated flexible plate with injection/suction and radiation was studied by Prabakaran et al. [6]. Mankiw et al. [7] analysed the MHD time-dependent flow of nanofluid with variable properties due to an inclined stretching sheet under thermal radiation. Shahid [8] studied the effect of an upper convective Maxwell fluid over a permeable surface near the stagnation point. Rafique et al. [9] addressed the stratified micropolar nanofluid flow past the Riga surface. The unsteady viscous flow of the nanofluid flow over the Riga plate using a rotating system was investigated by Parvine et al. [10]. Abbas et al. [11] studied entropy production over the Riga plate with the suction case. Mohamed et al. [12] using a non-homogeneous dynamic model, which is physically more accurate in describing nanofluids than homogeneous ones. They numerically examined the free convective flow in a cubical cavity filled with a copper–water nanofluid. Aziz et al. [13] discussed the characteristics of nanoparticles with Lorentz and Coriolis forces. More developments of nanofluids are in [14–17].

Different fluid forms, such as polymer melts, colloidal suspensions and organic chain mixes, are used in a wide range of industrial and production processes. The rheological behaviour of these fluids cannot be described well by the Naiver–Stokes equation. Therefore, several nonlinear fluid models have been proposed to represent the rheological characteristics of complicated fluids. One of the non-Newtonian fluid models is used to examine the key characteristics of pseudoplastic and dilatant fluids, which is known as Sutterby fluid model. Numerous experts have studied the flow of the Sutterby liquid extensively. Waqas et al. [18] inspected the Sutterby nanofluid flow using two rotating disks. Yahya et al. [19] investigated Williamson Sutterby nanoparticles under the Cattaneo–Christov heat flux. The effect of MHD on Sutterby nanoparticles due to porous movable sheets was discovered by Fayydh et al. [20]. Gowda et al. [21] examined the Cattaneo–Christof theory of heat diffusion in a Sutterby nanofluid. The thermal aspect of Sutterby nanofluid containing the microorganisms due the stretched cylinder was examined by Aldabesh et al. [22]. Hayat et al. [23] investigated the Sutterby fluid with thermal radiation due to a rotating disk. Fujii et al. [24] addressed a Sutterby fluid with natural convection flow due to a vertical plate. Darcy surface with MHD flow of Sutterby fluid was reported by Bilal et al. [25]. The bioconvection flow of a Sutterby nanofluid due to a rotating disk is described by Khan et al. [26]. Sohail et al. [27] designed the free convection flow of a Sutterby fluid with Cattaneo–Christov theory. The heat generation/absorption in the thermally stratified flow of a Sutterby fluid through a linearly stretched plate is analysed by Saif et al. [28]. Usman et al. [29] investigated the two-dimensional stagnant flow of a Sutterby nanofluid across a stretching wedge with porous media. Ali et al. [30] discussed the heat and mass transportation of a Sutterby nanofluid due to a horizontally stretching surface with bioconvection of microorganisms. The influence of homogeneous–heterogeneous reaction on Sutterby fluid flow through a disk with Cattaneo–Christov heat flux was studied by Khan et al. [31].

In the modern period, research on bioconvection exists due to the upwards motion of microorganisms, whose microorganisms are denser than water. The upward surface of the fluid develops thickness due to the collection of the microorganisms. Because of this, the upper surface becomes disturbed and microorganisms are fall down, which develops the bioconvection. Bioconvection phenomena have been continuously researched due to their applications in the clinical area, manufacturing process and biofuel production. Bioconvection can be organised in the motion of direction with enormous microorganism species. In this way, gyrotactic microorganisms are among those whose swimming directional is based on viscous and gravitational force. Kuznetsov et al. [32,33] reported the investigation of bioconvection in a mixed suspension of nanoparticles with gyrotactic microorganisms. Kotha et al. [34] examined the MHD flow of nanofluids with motile gyrotactic microorganisms over a vertical plate. Siddiq et al. [35] analysed numerically, through the bvp4c method, the bioconvection of micropolar nanofluid flow through a stretchable

disk. Ali et al. [36] studied the effect of bioconvection and Cattaneo–Christov heat flux effects of a micropolar-type nanofluid past a vertical stretching sheet. Azam et al. [37] investigated the effect of bioconvection flow for a Sutterby nanoliquid with nonlinear radiation. Khashi'ie et al. [38] studied a hybrid nanofluid having bioconvection with gyrotactic microorganisms. Azam [39] explored the time-dependent flow of the chemically reactive Sutterby nanofluid and the influence of gyrotactic microorganisms. Hayat et al. [40] operated the bioconvection flow of nanomaterial subject to the melting effect. They addressed thermal nonlinear radiation and Joule heating for heat distribution characteristics. Reddy et al. [41] analysed the time-dependent flow of a cross nanofluid comprising the gyrostatic microorganisms due to slip velocity. Sarkar et al. [42] defined a Sutterby nanofluid flow having motile gyrotactic microorganisms over the Riga plate. Syed et al. [43] described the biocovective phenomena of a Prandtl hybrid nanofluid over a stretched surface.

The current investigation aims to express the Sutterby nanofluid flow over a Riga plate with Cattaneo–Christov double diffusion and gyrotactic microorganisms. Chemical reactions and heat source-sink are considered. The main intention of this work is the inclusive analysis of this flow problem. The governing systems are designed as a coupled partial system. The flow problems are altered into the nonlinear ordinary system by applying suitable transformations. Further, the solution of ordinary differential equations is computed via the homotopy analysis method (HAM). The novel outcomes of the current work are obtained through different parameters and explained in detail with graphs and tables.

2. Description of the Physical Model

Consider the incompressible and steady flow of a Sutterby nanofluid over the Riga plate containing gyrotactic microorganisms. Cattaneo–Christov with heat and mass flux were also incorporated into the temperature and concentration equation. The x-axis is considered along with the sheet and the y-axis is taken perpendicular to the sheet. Moreover, the velocity of the sheet is taken as $U_w = ax$. The temperature of the surface, the concentration of the surface and the microorganism of the surface are represented by T_w, C_w and χ_w, respectively. Furthermore, it was assumed that the fluid contains gyrotactic bacteria. The fluids' microorganisms gravitate towards the light. Gyrotactic phenomena, or movement against gravity, are made possible by the "bottom heavy" bulk microorganism, which orients their bodies. The existence of microorganisms is advantageous for the suspension of the nanoparticles. The motion of microorganisms is taken, irrespective of that of the nanoparticles, to ensure the stability of convection. The flow of a double-diffusive fluid across a Riga plate containing gyrotactic microorganisms has not been investigated, and this study aims to fill that gap with the simplification of unsteady boundary layer approximation expressions provided in [22]. Figure 1 describes the physical model of the present problem.

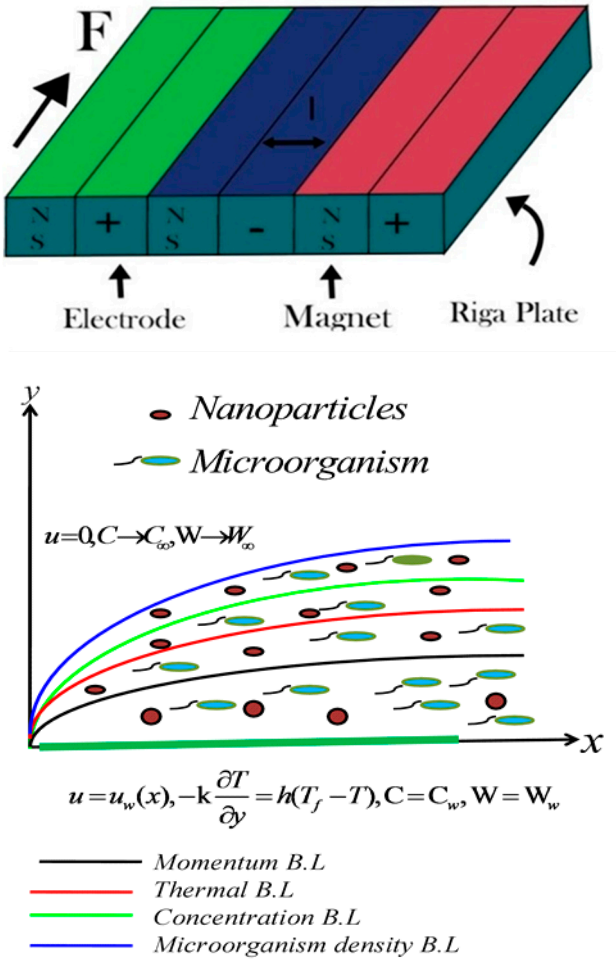

Figure 1. Physical configuration of the flow problem.

Fluid Model

The Cauchy stress tensor τ for the Sutterby fluid [44] is defined as

$$\tau = \mu(\dot{\gamma})A_1 - pI, \tag{1}$$

where the Sutterby viscosity model is represented as

$$\mu = \mu_\circ \left[\left(\frac{\sinh^{-1}\left(\dot{\beta}\dot{\gamma}\right)}{\left(\dot{\beta}\dot{\gamma}\right)} \right) \right]^n, \tag{2}$$

where n, $\mu_\circ$ and $\dot{\beta}$ are the power law index, zero share rate viscosity and time material constant.

Introducing Equation (2) into Equation (1), then we have

$$\tau = \mu_\circ \left[\left(\frac{\sinh^{-1}\left(\dot{\beta}\dot{\gamma}\right)}{\left(\dot{\beta}\dot{\gamma}\right)} \right) \right]^n A_1 - p. \tag{3}$$

The governing equations are illustrated in the following form [21]:

$$\frac{\partial u}{\partial x} + \frac{\partial v}{\partial y} = 0 \tag{4}$$

$$u\frac{\partial u}{\partial x}+v\frac{\partial u}{\partial y}=\frac{\mu_0}{\rho}\left[\frac{\partial^2 u}{\partial y^2}+\frac{\beta B^2}{2}\left(\frac{\partial u}{\partial y}\right)^2\frac{\partial^2 u}{\partial y^2}\right]+\frac{\pi j_0 M_0}{8\rho}\exp\left(-\frac{\pi}{d}y\right) \tag{5}$$

$$u\frac{\partial T}{\partial x}+v\frac{\partial T}{\partial y}+\Phi_E\Omega_E=\frac{k}{\rho C_p}\left(\frac{\partial^2 T}{\partial y^2}\right)+\tau\left(D_B\frac{\partial C}{\partial y}\frac{\partial T}{\partial y}+\frac{D_T}{T_\infty}\left(\frac{\partial T}{\partial y}\right)^2\right)-\frac{1}{\rho C_p}\frac{\partial q_r}{\partial y}+\frac{Q_0}{\rho C_p}(T-T_\infty), \tag{6}$$

$$u\frac{\partial C}{\partial x}+v\frac{\partial C}{\partial y}+\Phi_C\Omega_C=D_B\frac{\partial^2 c}{\partial y^2}+\frac{D_T}{T_\infty}\left(\frac{\partial^2 T}{\partial y^2}\right)-K_0(C-C_\infty), \tag{7}$$

$$u\frac{\partial \chi}{\partial x}+v\frac{\partial \chi}{\partial y}+\frac{b\chi_c}{(C_w-C_\infty)}\frac{\partial}{\partial y}\left(\chi\frac{\partial C}{\partial y}\right)=D_m\frac{\partial^2 \chi}{\partial y^2}, \tag{8}$$

where u and v are velocity components in the x and y directions. v represents the kinematic viscosity of the fluid, ρ represents the density of the fluid, α represents the thermal diffusivity, C is the concentration, D_B and D_t represent Brownian diffusion and thermophoretic diffusion (respectively), C_p denotes volumetric expansion, D_m represents microorganism coefficient, and Ω_E and Ω_C are the fluid relaxation time.

In the above equations, the terms Ω_E and Ω_C are stated as

$$\Omega_E=u\frac{\partial u}{\partial x}\frac{\partial T}{\partial x}+v\frac{\partial u}{\partial y}\frac{\partial T}{\partial x}+u\frac{\partial v}{\partial x}\frac{\partial T}{\partial y}+v\frac{\partial v}{\partial y}\frac{\partial T}{\partial y}+u^2\frac{\partial^2 T}{\partial x^2}+2uv\frac{\partial^2 T}{\partial x\partial y}+v^2\frac{\partial^2 T}{\partial y^2} \tag{9}$$

$$\Omega_C=u\frac{\partial u}{\partial x}\frac{\partial C}{\partial x}+v\frac{\partial u}{\partial y}\frac{\partial C}{\partial x}+u\frac{\partial v}{\partial x}\frac{\partial C}{\partial y}+v\frac{\partial v}{\partial y}\frac{\partial C}{\partial y}+u^2\frac{\partial^2 C}{\partial x^2}+2uv\frac{\partial^2 C}{\partial x\partial y}+v^2\frac{\partial^2 C}{\partial y^2} \tag{10}$$

The relevant boundary conditions are assumed to be:

$$\left.\begin{array}{l} u=u_w(x),\ v=0,-k\frac{\partial T}{\partial y}=h(T_w-T_\infty),\ C=C_w,\ \chi=\chi_w\ as\ y=0,\\ u\to 0,\ T\to T_\infty,\ C\to C_\infty,\ \chi\to\chi_\infty\ at\ y\to\infty. \end{array}\right\} \tag{11}$$

$$q_r=\frac{4\sigma_1}{3k^*}\frac{\partial T^4}{\partial y}=-\frac{16\sigma^*}{3k^*}T^3\frac{\partial T^4}{\partial y}, \tag{12}$$

where T^4 can be expanded as follows:

$$T^4\ \cong 4T^3{}_\infty T-3T^4{}_\infty. \tag{13}$$

Replacing Equation (12) into Equation (13),

$$q_r=\frac{16\sigma * T^3{}_\infty}{3k^*}\frac{\partial T}{\partial y}. \tag{14}$$

Introducing the variables [14]

$$\left.\begin{array}{l} u=axf'(\eta), v=-\sqrt{a\upsilon}f(\eta), \eta=y\sqrt{\frac{a}{\upsilon}},\\ \theta=\frac{T-T_\infty}{T_w-T_\infty}, \phi=\frac{C-C_\infty}{C_w-C_\infty}, W=\frac{\chi-\chi_\infty}{\chi_w-\chi_\infty}, \end{array}\right\} \tag{15}$$

Using Equation (15), Equations (4)–(6) become

$$f'''+f\,f''-f'^2+\frac{1}{2}\beta\delta Re_\gamma f''^2 f'''+Ze^{-A\eta}=0, \tag{16}$$

$$\theta''\left(1+\frac{4}{3}Rd\right)+\mathrm{Pr}Nt\,\theta'^2+\mathrm{Pr}Nb\,\theta'\phi'-\mathrm{Pr}\lambda_1\left(ff'\theta'+f^2\theta''\right)+\mathrm{Pr}\Upsilon\theta=0 \tag{17}$$

$$\phi''+Scf\phi'+\left(\frac{Nt}{Nb}\right)\theta''-\mathrm{Pr}Sc\lambda_2\left(ff'\phi'+f^2\phi''\right)-ScCr\phi=0, \tag{18}$$

$$W''-Pe\left[\phi''(W+\varpi)+\phi'W'\right]-LbfW'=0, \tag{19}$$

The corresponding boundary conditions are

$$\left.\begin{array}{l} f(0)=0, f'(0)=1, \theta'(0)=Bi(\theta(0))-Bi, \phi(0)=1 \\ f'(\infty)=0, \theta(\infty)=0, \phi(\infty)=0, W(\infty)=0. \end{array}\right\} \tag{20}$$

where $Z=\frac{\pi J_\circ M_\circ h}{8\rho U_\circ^2}$ is the modified Hartmann number; $Re_\gamma=\frac{ax^2}{v}$ is the Reynolds number; $\delta=\frac{B^2a^2}{v}$ is the Deborah number; $Rd=\frac{4\sigma^* T_\infty^3}{kk^*}$ is the radiation parameter; $\Pr=\frac{v}{a}$ is the Prandtl number; $Nb=\frac{\tau D_B(C_w-C_\infty)}{v}$ is the Brownian motion parameter; $Nt=\frac{\tau D_t(T_w-T_\infty)}{T_\infty v}$ is the thermophoresis parameter; $Sc=\frac{v}{D_B}$ is the Schmidt number; $Bi=\frac{h_f}{k}\sqrt{\frac{v}{a}}$ is the Biot number; $Pe=\frac{bW_c}{D_m}$ is the Peclet number; $Lb=\frac{v}{Dm}$ is the bioconvection Lewis number; and $Cr=\frac{K_\circ}{c}$ is the chemical reaction.

The thermofluidic quantities of engineering interest in this study are skin friction, Cf_x, heat transfer rate, Nu_x, mass transfer rate, Sh_x, and motile density, Wh_x.

$$\left.C_{fx}=\frac{\tau_w}{pu_w^2}, Nu_x=\frac{xq_w}{k(T_w-T_\infty)}, Sh_x=\frac{xq_m}{D_b(C_w-C_\infty)} \text{ and } Wh_x=\frac{xq_n}{D_m(X_w-X_\infty)}\right\} \tag{21}$$

where τ_w is the surface shear stress, q_w is the surface heat flux, q_m is the surface mass flux and q_n is the motile density, which are presented by the following expressions:

$$\left.\begin{array}{l} \tau_w=-\mu_0\left[\frac{\partial u}{\partial y}+\frac{1}{6}\beta\delta Re_\gamma\left(\frac{\partial u}{\partial y}\right)^3\right]_{y=0}, q_w=-k\left(\frac{\partial T}{\partial y}\right)\Big|_{y=0}, \\ q_m=-k\left(\frac{\partial C}{\partial y}\right)\Big|_{y=0} \text{and } q_n=-D_m\left(\frac{\partial \chi}{\partial y}\right)\Big|_{y=0}. \end{array}\right\} \tag{22}$$

The dimensionless form of the above parameters is expressed as

$$\left.\begin{array}{l} C_{fx}Re_x^{0.5}=\left[f''(0)+\frac{1}{6}\beta\delta Re_\gamma(f''(0))^3\right], \frac{Nu_x}{Re_x^{1/2}}=-\left[1+\frac{4}{3}Rd\right]\theta'(0), \\ \frac{Sh_x}{Re_x^{1/2}}=-\phi'(0) \text{ and } \frac{Wh_x}{Re_x^{1/2}}=-W'(0). \end{array}\right\} \tag{23}$$

where $Re_x=\frac{xU_w}{v}$ is the local Reynolds number.

3. Entropy Generation Analysis

The entropy generation with a Sutterby nanofluid is communicated as [37]:

$$\begin{array}{l} S_{gen}'''=\frac{k}{T_\circ}\left(\left[\frac{\partial T}{\partial x}\right]^2+\left[\frac{\partial T}{\partial y}\right]^2+\frac{16\sigma^* T_\infty^3}{3kk^*}\left(\frac{\partial T}{\partial y}\right)^2\right)+\frac{\mu}{T_\infty}\left(\frac{\partial u}{\partial y}\right)^2\left[1+\frac{\beta\delta Re_\gamma}{6}\left(\frac{\partial u}{\partial y}\right)^2\right] \\ +\frac{RD_m}{C_\infty}\left(\frac{\partial C}{\partial y}\right)^2+\frac{RD_m}{T_\infty}\left(\frac{\partial T}{\partial y}\right)\left(\frac{\partial C}{\partial y}\right)+\frac{RD_m}{\chi_\infty}\left(\frac{\partial \chi}{\partial y}\right)^2+\frac{RD_m}{T_\infty}\left(\frac{\partial \chi}{\partial y}\right)\left(\frac{\partial T}{\partial y}\right). \end{array} \tag{24}$$

The significance of the entropy production can be written as

$$S_\circ'''=\frac{\kappa(\Delta T)^2}{L^2T_\infty^2} \tag{25}$$

Using Equation (15), the rate of entropy Equation (24) can be converted as:

$$\begin{array}{l} N_G=\frac{S_{gen}'''}{S_\circ'''}=Re_\gamma(1+Rd)\theta'^2+Re_\gamma\frac{Br}{\Pi}\left[1+\frac{\beta\delta Re_\gamma}{3}(f'')^2\right]+Re_\gamma\left(\frac{\Gamma}{\Pi}\right)^2\phi'^2 \\ +Re_\gamma\left(\frac{\Gamma}{\Pi}\right)\phi'\theta'+Re_\gamma\left(\frac{\xi}{\Pi}\right)^2W'^2+Re_\gamma\left(\frac{\xi}{\Pi}\right)W'\theta'. \end{array} \tag{26}$$

The Bejan number Be is defined as the ratio over the entropy generation with heat transport, S_T, and the total entropy production, N_G, and it can be written as:

$$\begin{aligned} Be &= \frac{S_T}{N_G} \\ Be &= \frac{Re_\gamma(1+Rd)\theta'^2+Re_\gamma\left(\frac{\Gamma}{\Pi}\right)^2\phi'^2+Re_\gamma\left(\frac{\Gamma}{\Pi}\right)\phi'\theta'+Re_\gamma\left(\frac{\xi}{\Pi}\right)^2W'^2+Re_\gamma\left(\frac{\xi}{\Pi}\right)W'\theta'}{Re_\gamma(1+Rd)\theta'^2+Re_\gamma\frac{Br}{\Pi}\left[1+\frac{\beta\delta Re_\gamma}{3}(f'')^2\right]+Re_\gamma\left(\frac{\Gamma}{\Pi}\right)^2\phi'^2} \\ &\quad +Re_\gamma\left(\frac{\Gamma}{\Pi}\right)\phi'\theta'+Re_\gamma\left(\frac{\xi}{\Pi}\right)^2W'^2+Re_\gamma\left(\frac{\xi}{\Pi}\right)W'\theta' \end{aligned} \tag{27}$$

4. Homotopy Expression

Nonlinearity issues are solved using a variety of numerical approaches. The HAM [45–52] technique, which is the most successful semi-analytically approach and applied to utilize these greatly nonlinear equations. These variables are used to calculate the approximation rate of this solution. The flow map of HAM process is given in Chart 1. Furthermore, the user can select the starting assumptions for the solutions. The higher order non-linear ODE Equations (16)–(20) are solved through this HAM technique.

$$f_\circ(\eta)=\left(1-e^{-\eta}\right),\theta_\circ(\eta)=\left[\frac{Bi}{1+Bi}\right]e^{-\eta},\phi_\circ(\eta)=e^{-\eta},W_\circ(\eta)=e^{-\eta}, \tag{28}$$

$$\hat{L}_f=f'''-f',\ \hat{L}_\theta=\theta''-\theta,\ \hat{L}_\phi=\phi''-\phi,\ \hat{L}_W=W''-W, \tag{29}$$

with the property

$$\left.\begin{aligned} &\hat{L}_f(R_1+R_2e^{-\eta}+R_3e^{-\eta})=0, \\ &\hat{L}_\theta(R_4+R_5e^{-\eta})=0, \\ &\hat{L}_\phi(R_6+R_7e^{-\eta})=0, \\ &\hat{L}_W(R_8+R_9e^{-\eta})=0, \end{aligned}\right\} \tag{30}$$

in which $Bi(i=1\text{–}9)$ are the constants.

Zeroth order formulation

$$\left.\begin{aligned} &(1-s)\hat{L}_f[f(\eta;s)-f_\circ(\eta)]=s\hbar_f N_{f}[f(\eta;s),\theta(\eta,s),\phi(\eta,s),W(\eta,s)], \\ &(1-s)\hat{L}_\theta[\theta(\eta;s)-\theta_\circ(\eta)]=s\hbar_\theta N_{\theta}[f(\eta;s),\theta(\eta,s),\phi(\eta,s)], \\ &(1-s)\hat{L}_\phi[\phi(\eta;s)-\phi_\circ(\eta)]=s\hbar_\phi N_{\phi}[f(\eta;s),\theta(\eta,s),\phi(\eta,s)], \\ &(1-s)\hat{L}_W[W(\eta;s)-W_\circ(\eta)]=s\hbar_W N_{W}[f(\eta;s),\theta(\eta,s),\phi(\eta,s)],W(\eta,s)]. \end{aligned}\right\} \tag{31}$$

$$\left.\begin{aligned} &f(0,s)=0,\ f'(0,s)=1,\ f'(\infty,s)=0, \\ &\theta'(0,s)=Bi[\theta(0,s)-1],\ \theta(\infty,s)=0, \\ &\phi(0,s)=1,\ \phi(\infty,s)=0, \\ &W(0,s)=0,\ W(\infty,s)=0, \end{aligned}\right\} \tag{32}$$

where N_{f}, N_{θ}, N_{ϕ} and N_{W} are defined below:

$$\begin{aligned} N_{f}[f(\eta,s)] &= \frac{\partial^3 f(\eta,s)}{\partial\eta^3}+f(\eta,s)\frac{\partial^2 f(\eta,s)}{\partial\eta^2}-\left[\frac{\partial f(\eta,s)}{\partial\eta}\right]^2 \\ &+\frac{1}{2}\beta\delta Re_\gamma\left[\frac{\partial f(\eta,s)}{\partial\eta}\right]^2\left[\frac{\partial^3 f(\eta,s)}{\partial\eta^3}\right]+Ze^{-A\eta}, \end{aligned} \tag{33}$$

$$N_{\theta}[f(\eta,s),\theta(\eta,s)] = \frac{\partial^2\theta(\eta,s)}{\partial\eta^2}\left(1+\frac{4}{3}Rd\right)+\Pr Nt\left[\frac{\partial\theta(\eta,s)}{\partial\eta}\right]^2 +\Pr Nb\left[\frac{\partial\theta(\eta,s)}{\partial\eta}\right]\left[\frac{\partial\phi(\eta,s)}{\partial\eta}\right]-\Pr\lambda_1\begin{pmatrix} f(\eta,s)\left[\frac{\partial f(\eta,s)}{\partial\eta}\right]\left[\frac{\partial\theta(\eta,s)}{\partial\eta}\right] \\ +[f(\eta,s)]^2\frac{\partial^2\theta(\eta,s)}{\partial\eta^2}\end{pmatrix} +\Pr\Upsilon\theta(\eta,s), \tag{34}$$

$$N_{\phi}[f(\eta,s),\theta(\eta,s),\phi(\eta,s)] = \frac{\partial^2\phi(\eta,s)}{\partial\eta^2}+Scf(\eta,s)\left[\frac{\partial\phi(\eta,s)}{\partial\eta}\right] +\left(\frac{Nt}{Nb}\right)\left[\frac{\partial^2\theta(\eta,s)}{\partial\eta^2}\right]-\Pr Sc\lambda_2\begin{pmatrix} f(\eta,s)\frac{\partial f(\eta,s)}{\partial\eta}\frac{\partial\phi(\eta,s)}{\partial\eta} \\ +f^2(\eta,s)\frac{\partial^2\phi(\eta,s)}{\partial\eta^2}\end{pmatrix}-ScCr\phi(\eta,s), \tag{35}$$

$$N_{W}[f(\eta,s),\phi(\eta,s),W(\eta,s),] = \frac{\partial^2W(\eta,s)}{\partial\eta^2}-Pe\begin{bmatrix}\frac{\partial^2\phi(\eta,s)}{\partial\eta^2}(W+\varpi) \\ +\frac{\partial\phi(\eta,s)}{\partial\eta}\frac{\partial W(\eta,s)}{\partial\eta}\end{bmatrix}-Lbf(\eta,s)\frac{\partial W(\eta,s)}{\partial\eta}. \tag{36}$$

For $s=0$ and $s=1$, the results are achieved:

$$\left.\begin{array}{l} f(\eta;0)=f_0(\eta),\ \theta(\eta;0)=\theta_0(\eta),\ \phi(\eta;0)=\phi_0(\eta),\ W(\eta;0)=W_0(\eta) \\ f(\eta;1)=f(\eta),\ \theta(\eta;1)=\theta(\eta),\ \phi(\eta;1)=\phi(\eta),\ W(\eta;1)=W(\eta)\end{array}\right\} \tag{37}$$

m^{th} order formulation

The m^{th} order deformation can be presented in the following forms:

$$\left.\begin{array}{l}\hat{L}_f[f_m(\eta,s)-\chi_m f_{m-1}(\eta)]=\hbar_f R_{f,m}(\eta), \\ \hat{L}_\theta[\theta_m(\eta,s)-\chi_m\theta_{m-1}(\eta)]=\hbar_\theta R_{\theta,m}(\eta), \\ \hat{L}_\phi[\phi_m(\eta,s)-\chi_m\phi_{m-1}(\eta)]=\hbar_\phi R_{\phi,m}(\eta), \\ \hat{L}_W[\theta_m(\eta,s)-\chi_m W_{m-1}(\eta)]=\hbar_W R_{W,m}(\eta).\end{array}\right\} \tag{38}$$

Boundary conditions are:

$$\left.\begin{array}{l} f'_m(0)=f_m(0)=f'_m(\infty)=\theta'_m(0)-Bi\theta_m(0)=\theta_m(\infty)=0, \\ \phi_m(0)=\phi_m(\infty)=W(0)=W(\infty)=0.\end{array}\right\} \tag{39}$$

where

$$R_{f,m}(\eta)=f'''_{m-1}(\eta)+\sum_{k=0}^{m-1}f_{m-1-k}f''_k-\sum_{k=0}^{m-1}f'_{m-1-k}f'_k+\frac{1}{2}\beta\delta Re_\gamma\sum_{k=0}^{m-1}f''_{m-1-k}f''_kf'''_k+Ze^{-A\eta} \tag{40}$$

$$R_{\theta,m}(\eta)=\theta''_{m-1}(\eta)\left(1+\frac{4}{3}Rd\right)+\Pr Nt\sum_{k=0}^{m-1}\theta'_{m-1-k}\theta'_k+\Pr Nb\sum_{k=0}^{m-1}\phi'_{m-1-k}\theta'_k -\Pr\lambda_1\left(\sum_{k=0}^{m-1}\left(\sum_{r=0}^{k}f_{m-1-k}f'_{k-r}\right)\theta'_k+\sum_{k=0}^{m-1}f'_{m-1-k}f'_k\theta''_k\right)+\Pr\Upsilon\theta_{m-1} \tag{41}$$

$$R_{\phi,m}(\eta)=\phi''_{m-1}(\eta)+Sc\sum_{k=0}^{m-1}f'_{m-1-k}\phi_k+\left(\frac{Nt}{Nb}\right)\theta''_{m-1} -\Pr Sc\lambda_2\left(\sum_{k=0}^{m-1}\left(\sum_{r=0}^{k}f_{m-1-k}f'_{k-r}\right)\phi'_k+\sum_{k=0}^{m-1}f'_{m-1-k}f'_k\phi''_k\right)-ScCr\phi_{m-1} \tag{42}$$

$$R_{W,m}(\eta)=W''_{m-1}(\eta)-Pe\left(\sum_{k=0}^{m-1}\phi''_{m-1-k}W_k+\phi''_{m-1}\varpi+\sum_{k=0}^{m-1}\phi'_{m-1-k}W'_k\right)- Lb\sum_{k=0}^{m-1}W'_{m-1-k}f_k \tag{43}$$

$$\eta_m=\left\{\begin{array}{l}0, m\le 1\\ 1, m>1\end{array}\right\}. \tag{44}$$

The general solutions are

$$\left.\begin{aligned} f_m &= f_m^* + R_1 + R_2 e^{\eta} + R_3 e^{-\eta} \\ \theta_m &= \theta_m^* + R_4 e^{\eta} + R_5 e^{-\eta} \\ \phi_m &= \phi_m^* + R_6 e^{\eta} + R_7 e^{-\eta} \\ W_m &= W_m^* + R_8 e^{\eta} + R_9 e^{-\eta} \end{aligned}\right\} \tag{45}$$

where f_m^*, θ_m^*, ϕ_m^*, W_m^* are the special solutions.

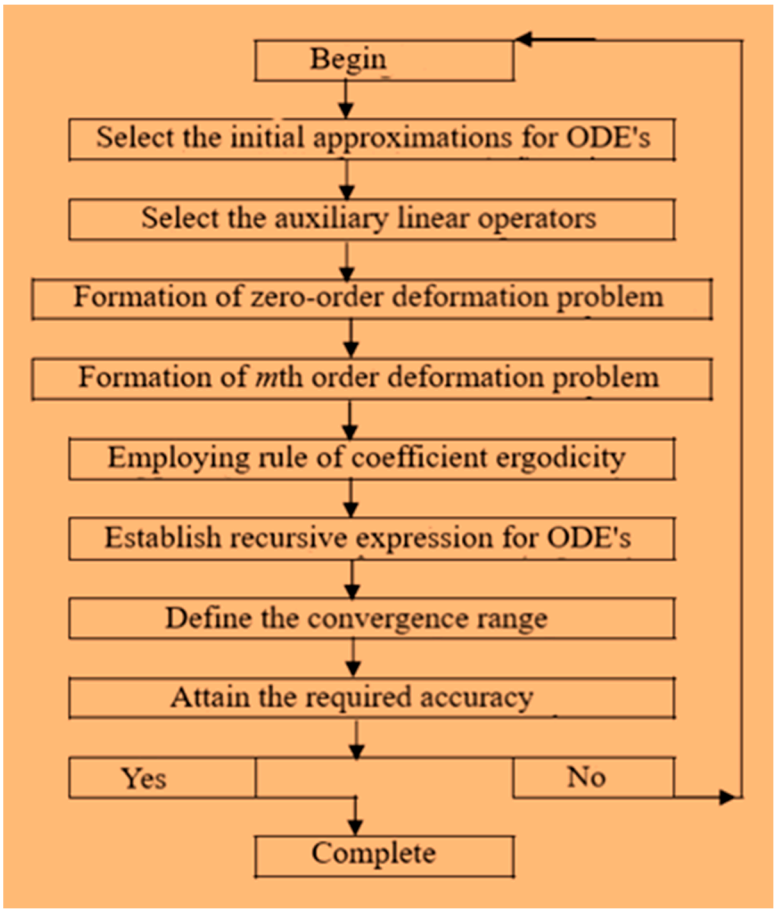

Chart 1. Flow chart of HAM expression.

Convergence of Homotopy Solutions

The parameters $\hbar_f, \hbar_\theta, \hbar_\phi$ and $\hbar_W$ are the converging control of the desired series solution. For the function $f''(0), \theta'(0), \phi'(0), W'(0)$ seek the permissible values to obtain the 25th and 30th order. Figures 1–4 specify that the range of $\hbar_f, \hbar_\theta, \hbar_\phi$ and $\hbar_W$ as $-2.0 < \hbar_f < -0.1, -2.0 < \hbar_\theta < -1.0, -1.7 < \hbar_\phi < -1.0$ and $-2.0 < \hbar_W < -1.0$. The series converges in the entire region of η when $\hbar_f = -0.65$, $\hbar_\theta = \hbar_\phi = -0.55$ and $\hbar_W = -0.7$. The order of approximation for HAM is denoted in Table 1.

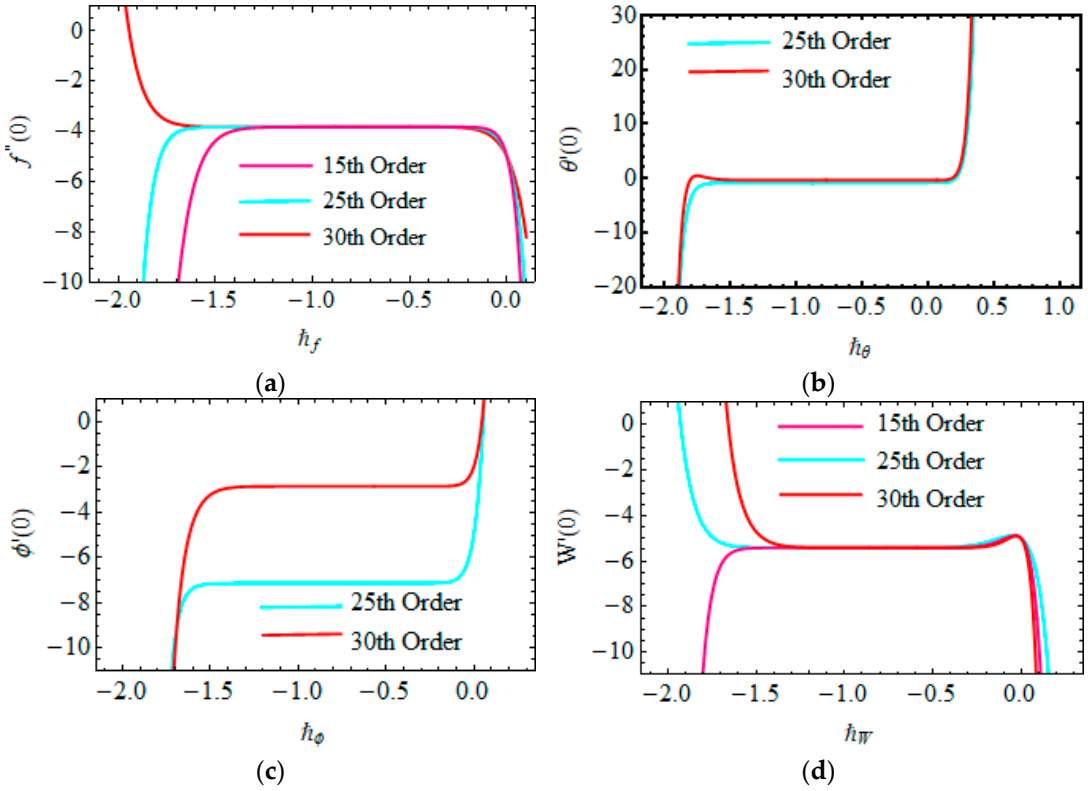

Figure 2. Plots of (**a**) $\hbar_f$—curve of $f''(0)$, (**b**) $\hbar_\theta$ —curve of $\theta'(0)$, (**c**) $\hbar_\phi$ —curve of $\phi'(0)$ and (**d**) $\hbar_w$ —curve of $W'(0)$.

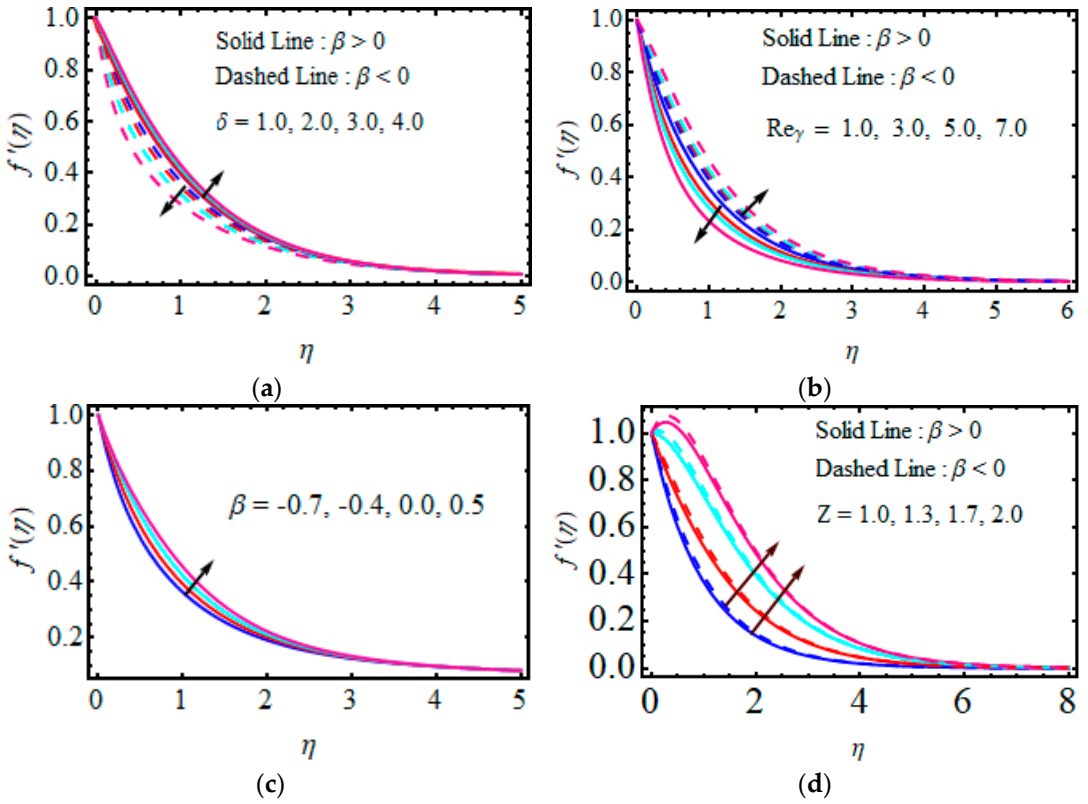

Figure 3. (**a**–**d**). The impact of the numerous variables of $f'(\eta)$: (**a**) δ, (**b**) Re_γ, (**c**) β and (**d**) Z.

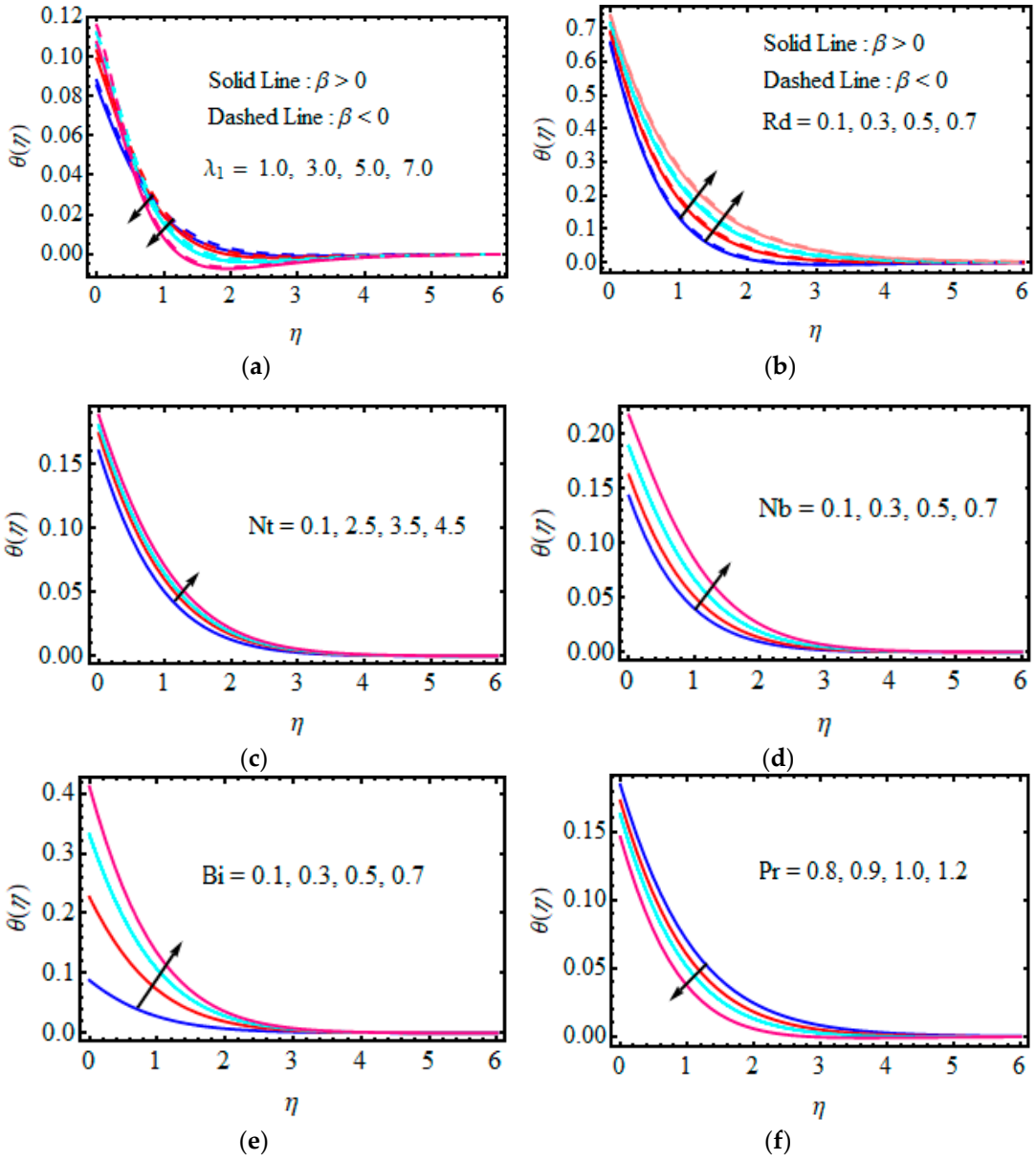

Figure 4. (**a**–**f**). The impact of the numerous variables of $\theta(\eta)$: (**a**) λ_1, (**b**) Rd, (**c**) Nt, (**d**) Nb, (**e**) Bi and (**f**) Pr.

Table 1. Convergence solution of HAM.

	Order of HAM			
Approximation	$-f''(0)$	$-\theta'(0)$	$-\phi'(0)$	$-W'(0)$
1	0.874702	0.166821	1.21667	0.955833
5	0.768677	0.167973	1.41759	1.038657
10	0.765186	0.168223	1.42596	1.07814
15	0.765357	0.168144	1.42606	1.08236
20	0.765347	0.168158	1.42609	1.08264
25	0.765341	0.168158	1.42608	1.08261
30	0.765341	0.168157	1.42608	1.08258
35	0.765341	0.168157	1.42608	1.08258
40	0.765341	0.168157	1.42608	1.08258

5. Results and Discussion

The system of Equations (16)–(19) subject to the boundary condition (20) was addressed through the homotopy analysis method (HAM). To discuss the performance of the physical significance against the velocity field $f'(\eta)$, temperature distribution $\theta(\eta)$, concentration field $\phi(\eta)$, motile microorganism profile $W(\eta)$, entropy production N_G, Bejan number Be, as well as skin friction, Nusselt number, Sherwood number and motile density microorganism were delineated, as seen in Figures 3–9. Table 2 verifies $-\theta(0)$ in accordance with Wang [52], Gorla and Sidawi [53], and Khan and Pop [54], with the limiting case $Nt = Nb = Rd = \lambda_1 = \Upsilon = 0$ and found a good agreement.

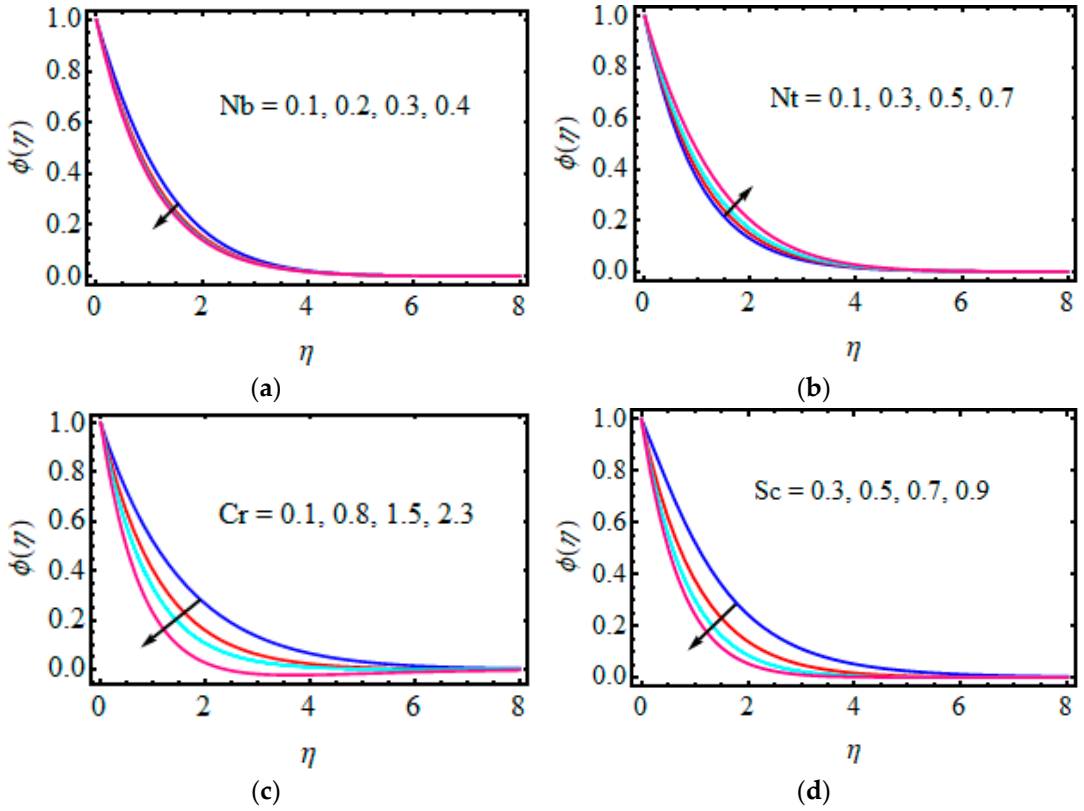

Figure 5. (**a**–**d**) The impact of the numerous variables of $\phi(\eta)$: (**a**), (**b**) Nt, (**c**) Cr and (**d**) Sc.

Table 2. Comparison of the obtained values of the Nusselt number $-\theta(0)$ with those of Wang [52], Gorla and Sidawi [53], and Khan and Pop 45 [54], when $Nt = Nb = Rd = \lambda_1 = \Upsilon = 0$.

Pr	Wang [52]	Gorla and Sidawi [53]	Khan and Pop [54]	Present
0.07	0.0663	0.0663	0.0663	0.0663
0.20	0.1691	0.1691	0.1691	0.1691
0.70	0.4539	0.4539	0.4539	0.4539
2.00	0.9113	0.9113	0.9113	0.9113

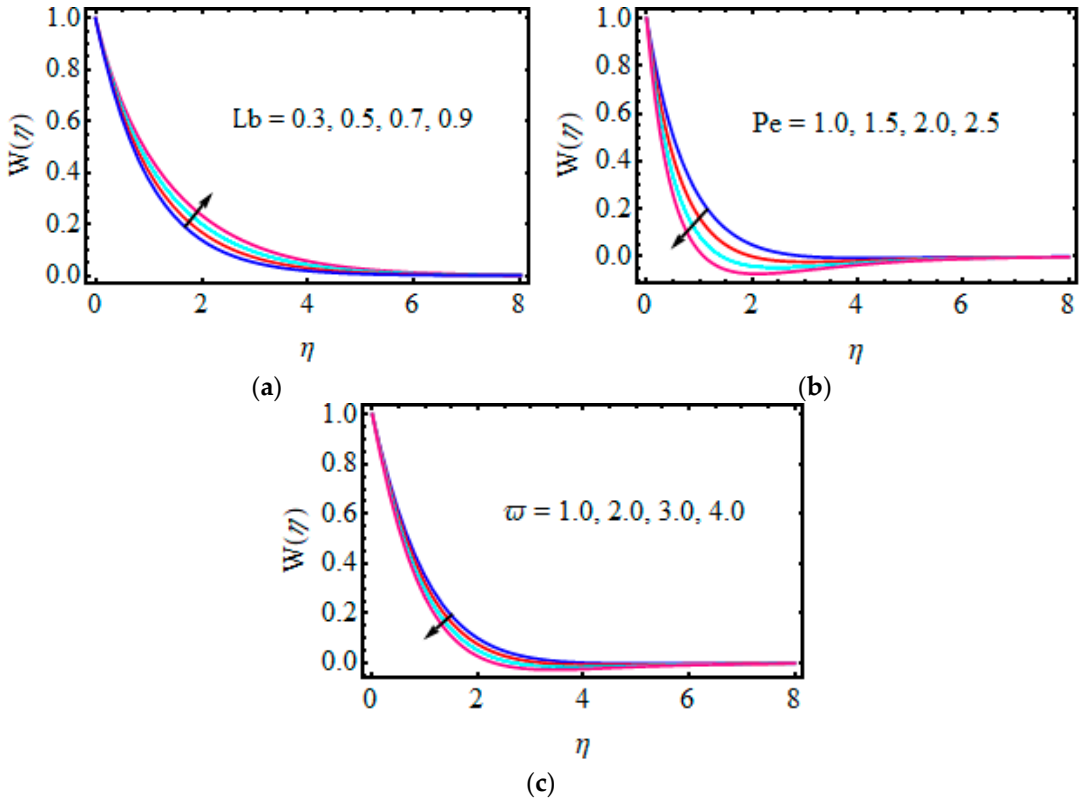

Figure 6. (**a**–**c**) The impact of the numerous variables of $\phi(\eta)$: (**a**) Nb, (**b**) Nb and (**c**) Cr.

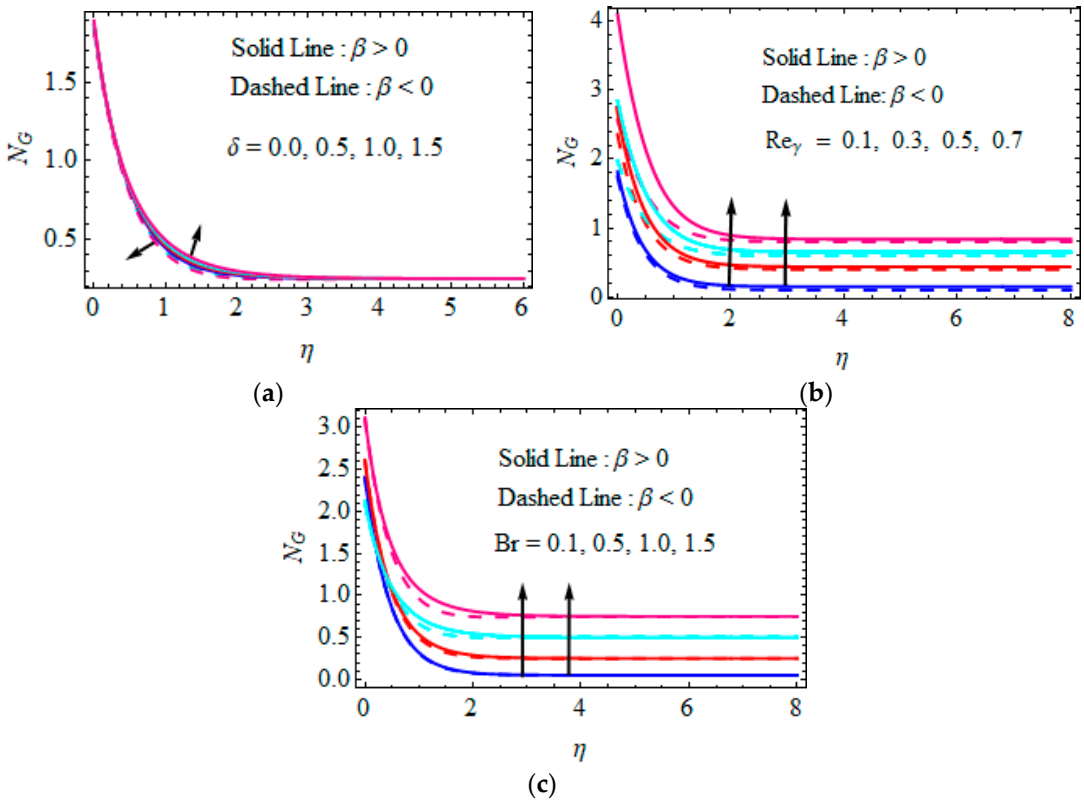

Figure 7. (**a**–**c**) The impact of the numerous variables of N_G: (**a**) δ, (**b**) Re_γ and (**c**) Br.

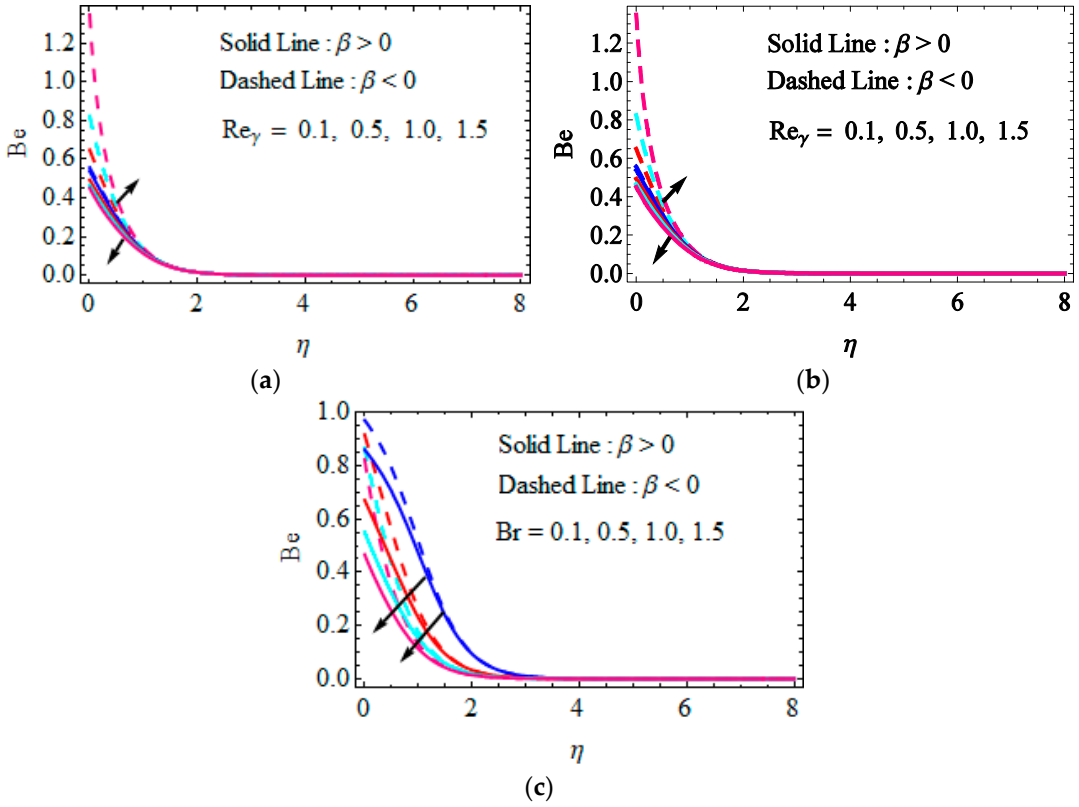

Figure 8. (**a**–**c**) The impact of the numerous variables of Be : (**a**) δ, (**b**) Re_γ and (**c**) Br.

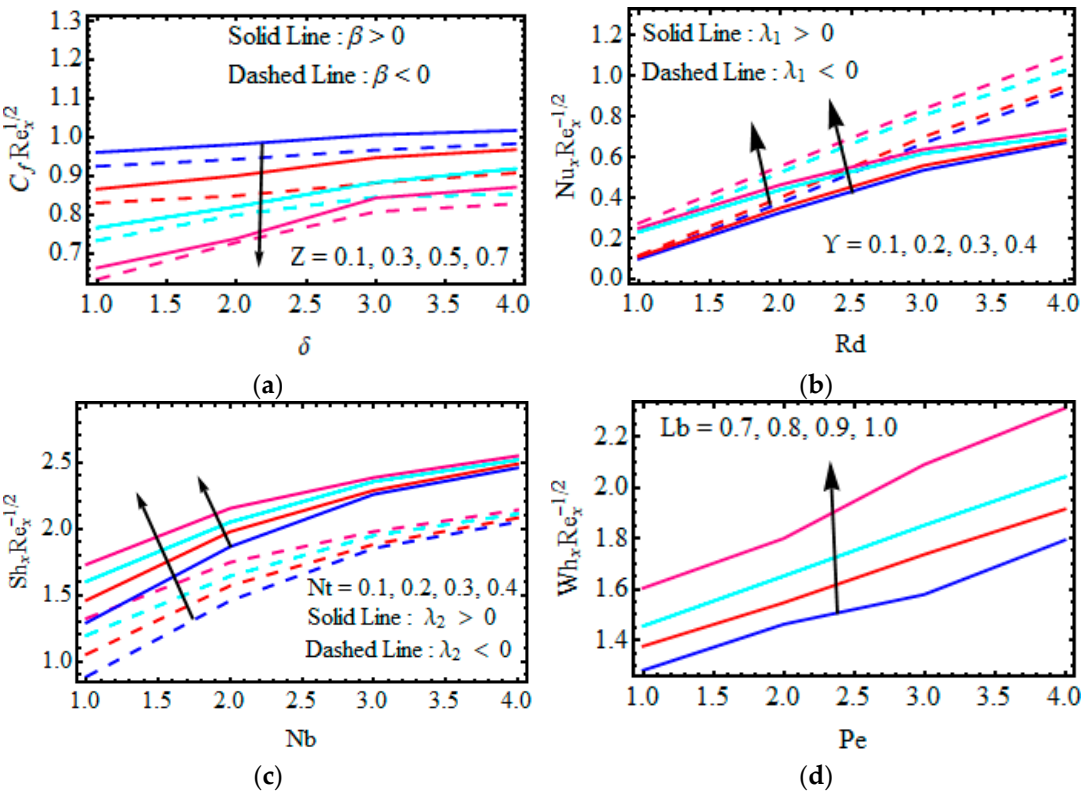

Figure 9. (**a**–**d**) Variation in the numerous variables of $Re_x^{1/2}Cf, Re_x^{-1/2}Nu, Re_x^{-1/2}Sh, Re_x^{-1/2}Wh_x$: (**a**) Z, δ, (**b**) Nb, Υ, (**c**) Nb, Nt and (**d**) Lb, Pe.

5.1. Velocity Profile

The effects of different numerous parameters over the velocity distribution $f'(\eta)$ are discussed in Figure 3a–d. Figure 3a shows that the velocity of the fluid diminishes with the superior values of Deborah number δ, for the case of $\beta < 0$, and the velocity field is enhanced for the rising value of Deborah number δ, for the case of $\beta > 0$. Figure 3b shows that the velocity field $f'(\eta)$ is reduced for higher Reynolds number Re_γ values, in the case of $\beta < 0$; a higher Re_γ tends to diminish the viscous force and the fluidity decreases for the pseudoplastic fluid. For shear thicking fluid, the velocity field enhances as Re_γ increases, for the $\beta < 0$ case. Figure 3c shows that the effect of the augmentation in the power law index parameter β causes that the velocity profile rises for shear thickening fluid. Figure 3d demonstrates the significance of the Hartmann number Z on the velocity field, for the two cases of $\beta < 0$ and $\beta > 0$. It was revealed that the strength of Z changes and the velocity of the fluid escalates in both cases. Physically, an increment in Z corresponds to enhancing the external electric field that constructs the wall-parallel Lorentz force. Therefore, $f'(\eta)$ increases.

5.2. Temperature Profile

Figure 4a–f plot the consequences of temperature $\theta(\eta)$ against different values of the involved parameters over the temperature field. The thermal relaxation time parameter impacts on $\theta(\eta)$ are demonstrated in Figure 4a. It can be noted that the thermal relaxation parameter tends to decrease the temperature profile for both the dilatants and pseudoplastic cases. Figure 4b reveals the inclination of $\theta(\eta)$ for specific values of the thermal radiation parameter, for $\beta > 0$ and $\beta < 0$. The temperature of the fluid increases due to the enlargement in the radiation parameter Rd in both cases. Figure 4c reports the variation of thermophoresis Nt over temperature. This is due to the nanoparticles move from the hotter surface to the colder surface. Figure 4d demonstrates the influence of the Brownian motion parameter Nb on the temperature profile. This is due to Brownian motion, which is the erratic movement of the particles suspended in the fluid. The random collision of particles suspended in the fluid increases the temperature of the fluid, which further contributes to the anticipated improvement in the temperature profile $\theta(\eta)$. Figure 4e depicts the impact of the Biot number $\theta(\eta)$. From the figure, it can be seen that the temperature field is boosted by enhancing the value of Bi. Actually, the Biot number Bi means the ratio of convection proportion of conducting the inner side of the boundary at the surface. Figure 4f displays variations of the Prandtl number against $\theta(\eta)$. The temperature is maintained in light of a higher Pr.

5.3. Nanoparticle Concentration Profile

The outcomes of the different leading parameters $\phi(\eta)$ are presented in Figure 5a–d. Figure 5a shows the characteristics of Nb on $\phi(\eta)$. The concentration distribution depletes with a rising Nb. Brownian motion's relationship with the Brownian diffusion coefficient, which causes the concentration field to decrease, is the cause of this phenomenon. The influence of the thermophoresis variable on $\phi(\eta)$ is rendered in Figure 5b. An augmentation in Nt leads to a reduction in concentration. One can notice, from that graph, the upsurge in Nt improves the mass transfer. The chemical reaction influences the profile of concentration, as seen in Figure 5c. The enhanced values Cr result in a fluid particle break near the surface, which reduces the concentration and the corresponding boundary layer thickness. The Schmidt number effect against the concentration profile is displayed in Figure 5d. Clearly, a depreciation in concentration is noted for the greater Sc, due to the reduction in mass diffusion.

5.4. Microorganism Profile

The effect of different influential variables on the microorganism's field is shown in Figure 6a–c. Variations in motile microorganisms against the biocovection Lewis number Lb for various values are seen in Figure 6a. Therefore, the greater values of Lb reduces

the microorganism field. Actually, Lb has an opposite trend with thermal diffusivity as an escalation in Lb decreases the thermal diffusivity in regards to a decline in motile density. From Figure 6b, it can be seen that the higher Peclet number in the microorganism field produces a reduction in $W(\eta)$. It has a direct relation with cell swimming speed; therefore, the climbing Pe improves the cell speed of micro-best stumbling microorganism diffusivity. As a result, $W(\eta)$ declines with the rising values of Pe. Figure 6c examines the characteristics of $W(\eta)$, the opposite ϖ. It can be seen that the motile density shrinks for the larger ϖ. In fact, improving the values of ϖ escalates the concentration of microorganisms in ambient concentration. Finally, $W(\eta)$ declines.

5.5. Entropy Generation Profile

Figure 7a–c examine the performance of numerous variable parameters δ, Re_γ and Br entropy production N_G. Figure 7a sketched the effect of Deborah number δ over N_G. This shows the enhancement in entropy production close to the wall for dilatant $\beta > 0$ and deduction close to the wall for pseudoplastic fluid $\beta < 0$. Increasing the influence in the Reynolds number Re_γ entropy generation is studied for dilatant and pseudoplastic fluid fluids plots in Figure 7b. The disparity in N_G against Br is plotted in Figure 7c. Entropy generation increases with increasing value Br in both cases. Subsequently, Br attributes the proportion of free heat through viscous heating with the molecular condition. Therefore, heat is created in the system for increased values of Br as well as disorder increasing in the system, which explains the upsurges in the entropy of the system.

5.6. Bejan Number Profile

The performance Be is opposite to the variations in the variables δ, Re_γ and Br; the plots Be are shown in Figure 8a–c. Figure 8a,b show the behaviour of the physical parameters of the Deborah and Reynolds numbers on the Bejan number. It examined that the Bejan number declines with the larger values of Deborah and Reynolds numbers for shear thickening and increases for both numbers for the shear-thinning fluid. Furthermore, Figure 8c shows that the influence of the Bejan number Be reduces ($\beta > 0, \beta < 0$) with the growing values of Br.

5.7. Physical Entitles

Figure 9a reports that the skin friction coefficient $Re_x^{1/2} Cf_x$ is deformed in both cases for the larger values of the parameters Z and δ for $\beta < 0$ and $\beta > 0$. The influence of the non-Newtonian nanofluid parameter on the Nusselt number $Re_x^{-1/2} Nu$ against the thermal radiation Rd is highlighted in Figure 9b. The heat transport gradient increases when rising the Rd and Υ. The significance of Nt and Nb on the Sherwood number is shown in Figure 9c. It is determined that there is amplification in the Sherwood number $Re_x^{-1/2} Sh$ for raised values of fluid parameters. Figure 9d elucidates the substantial rescaled density number of motile microorganisms. The rescaled density number of motile microorganisms is voluminous for higher variations of Pe and Lb. Figure 10a–d shows the 3D representation of skin friction, Nusselt number, Sherwood number and motile density, respectively.

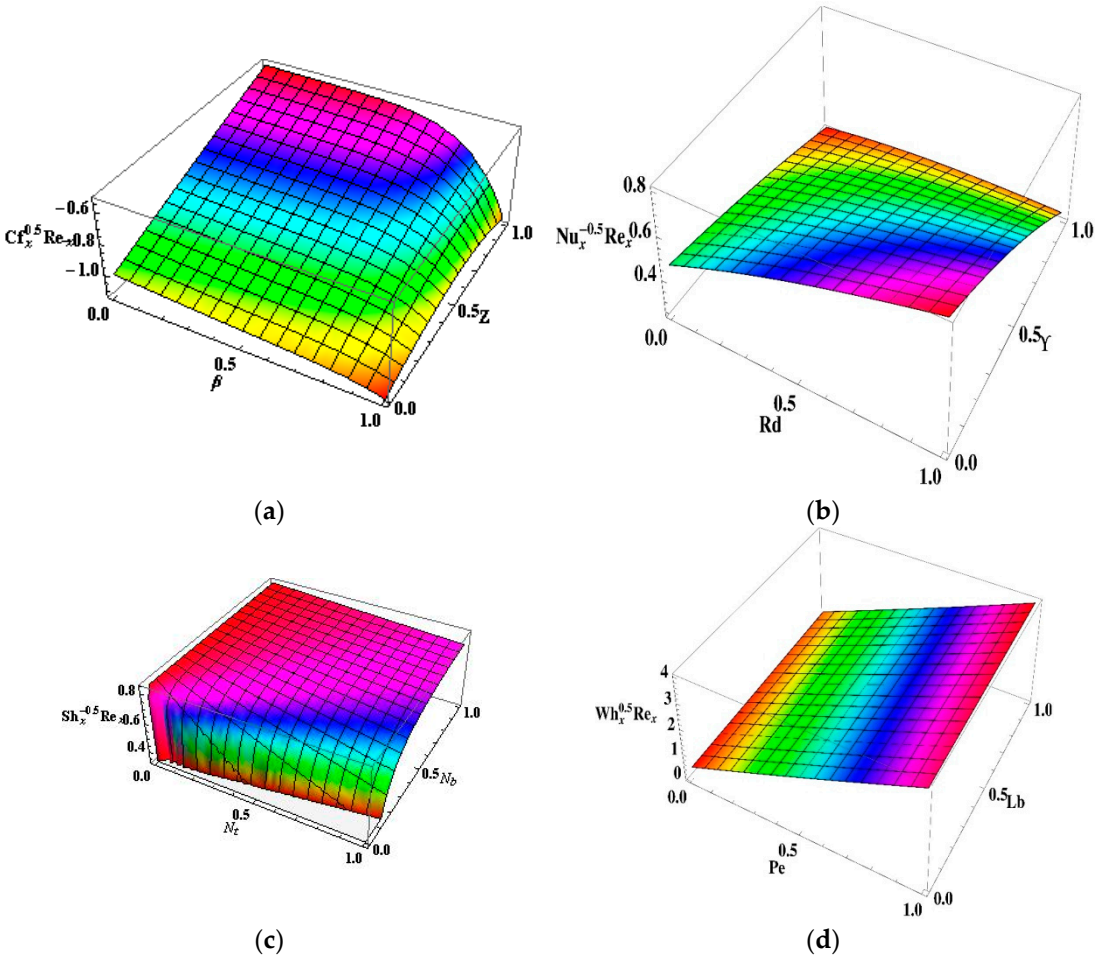

Figure 10. (**a**–**d**) Three-dimensional graphs; (**a**) Skin friction for β and Z; (**b**) Nusselt number for Rd and Υ; (**c**) Sherwood number for Nt and Nb; and (**d**) motile density for Pe and Lb.

5.8. Stream Line and Isotherm Line

Figure 11b shows the behaviour of the stream function for the current flow. The patterns depict that the streamlines are more obscured and split into two sections, pseudo-plastic $\beta < 0$ and dilatant $\beta > 0$; the shape is modest and fills the flow field. Figure 12a,b show the behaviour of the isotherm line for the present flow for both the cases.

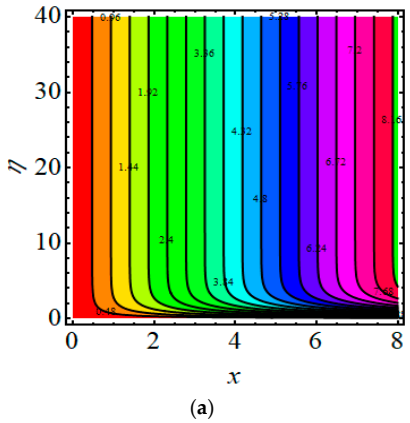

Figure 11. *Cont.*

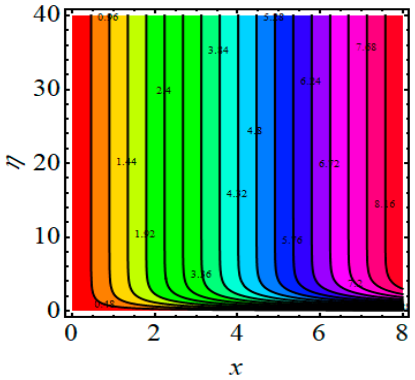

(**b**)

Figure 11. (**a**,**b**) Streamline for (**a**) $\beta = -2.5$ and (**b**) $\beta = 2.5$.

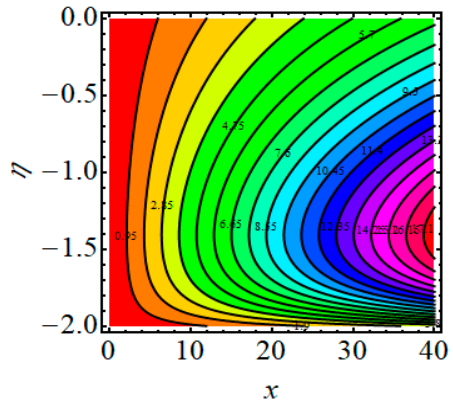

(**a**)

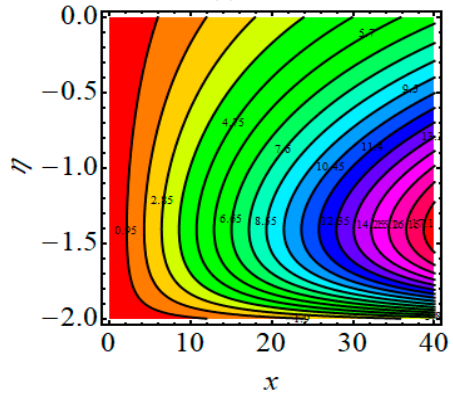

(**b**)

Figure 12. (**a**,**b**) Isotherm lines (**a**) $\beta = -2.5$ and (**b**) $\beta = -2.5$.

6. Major Outcomes

This investigation examined a Sutterby nanofluid with Cattaneo–Christov double diffusion theory over a Riga plate. Additionally, the bioconvection of the motile microorganisms and the chemical reaction was included. To obtain a non-linear system of ordinary differential problems, appropriate transformations were used. The non-linear systems were computed through the HAM technique. The main findings of the present study were as follows:

- The Deborah and Reynolds numbers produce the opposite behaviour in the flow field for the different cases of $\beta = -2.5$ and $\beta = 2.5$.
- The velocity shows the continuous improvement with increasing the Hartman number in both dilatant and pseudoplastic fluid cases.

- A larger chemical reaction reveals a decrement in the concentration, while the thermophoresis parameter Nt lead to the expansion in concentration.
- The microorganism field deteriorated for the higher values of Pe and microorganism difference parameter.
- The entropy generation number presented an increasing magnitude for large valuesof the Reynolds and Brinkman numbers, for the cases of pseudoplastic and dilatants fluid. Large values of entropy generation number appear in the area of the sheet due to the high viscous effects.
- Enhancing the value of the Deborah and Reynolds numbers results in the decrease in the Bejan profile in the case of the dilatant fluid, while the opposite effect is observed in the case of shear thinning.

Author Contributions: Conceptualization: M.F. and S.I.A.; Data curation: A.Z.; Formal analysis: M.F. and A.Z.; Investigation: F.A., K.L., A.Z. and S.I.A.; Methodology: K.L. and C.A.R.; Resources: M.F. and F.A.; Software: M.F. and K.L.; Supervision: S.I.A.; Validation: F.A. and S.I.A.; Visualization: C.A.R.; Writing—original draft: F.A., K.L. and M.F.; Writing—review and editing: C.A.R. and S.I.A. All authors have read and agreed to the published version of the manuscript.

Funding: This research received no external funding.

Data Availability Statement: Not applicable.

Acknowledgments: Sara I. Abdelsalam expresses her deep gratitude to Fundación Mujeres por África for supporting this work through the fellowship awarded to her in 2020.

Conflicts of Interest: The authors declare no conflict of interest.

Nomenclature

a	Stretching rate
f	Similarity function for velocity
T_∞	Ambient temperature
T	Fluid temperature
χ	Microorganism concentration
θ	Dimensionless temperature
C_∞	Ambient concentration
β	Power index number
δ	Deborah number
Re_γ	Local Reynolds number
Z	Modified Hartmann number
Rd	Thermal radiation
Υ	Heat source/sink parameter
Cr	Chemical reaction
λ_1	Thermal relaxation parameter
λ_2	Concentration relaxation parameter
Nt	Thermophoresis parameter
Nb	Brownian motion parameter
Bi	Biot number
Pr	Prandtl number
Sc	Schmidt number
Pe	Peclet number
Lb	Lewis number

ϖ	Microorganism concentration difference parameter
ρ	Fluid density
μ	Dynamic viscosity
∞	Ambient condition
C_f	Skin friction coefficient
Nu_x	Nusselt number
Sh_x	Sherwood number
Wh_x	Microorganism density number
τ	Ratio of the effective heat capacity
Br	Brinkman number
S_G	Local volumetric entropy generation rate
N_G	Entropy number
Be	Bejan number

References

1. Choi, S.U.; Eastman, J.A. Enhancing thermal conductivity of fluids with nanoparticles. in development and applications of non-Newtonian flow. *ASME* **1995**, *66*, 99–105.
2. Buongiorno, J. Convective transport in nanofluids. *J. Heat Transf.* **2006**, *128*, 240–250. [CrossRef]
3. Hussain, S.; Ahmad, S.; Mehmod, K.; Sagheer, M. Effects of inclintion angle on mixed convetive nanofluid flow in a double lid-driven cavity with discrete heat sources. *Int. J. Heat Mass Transf.* **2017**, *106*, 847–860. [CrossRef]
4. Hussain, S.; Ahmed, S.E.; Saleem, F. Impact of periodic magnetic field on entropy generation and mixed convection. *J. Thermophys. Heat Transf.* **2018**, *32*, 999–1012. [CrossRef]
5. Haq, F.; Saleem, M.; Rahman, M.U. Investigation of natural bio-convective flow of cross nanofluid containing gyrotactic microorganisems subject to activation energy and magnetic field. *Phys. Scr.* **2020**, *95*, 105219. [CrossRef]
6. Prabakaran, R.; Eswaramoorthi, S.; Loganathan, K.; Sarris, I.E. Investigation on Thermally Radiative Mixed Convective Flow of Carbon Nanotubes/Al_2O_3 Nanofluid in Water Past a Stretching Plate with Joule Heating and Viscous Dissipation. *Micromachines* **2022**, *13*, 1424. [CrossRef]
7. Mjankwi, M.A.; Masanja, V.G.; Mureithi, E.W.; James, M.N. Unsteady MHD flow of nanofluid with variable properties over a stretching sheet in the presence of thermal radiation and chemical reaction. *Int. J. Math. Math. Sci.* **2019**, *2019*, 7392459.
8. Shahid, A. The effectiveness of mass transfer in the MHD upper-convected Maxwell fluid flow on a stretched porous sheet near stagnation point: A numerical invstigation. *Inventions* **2020**, *5*, 64. [CrossRef]
9. Rafique, K.; Alotaibi, H.; Ibrar, N.; Khan, I. Stratified flow of micropolar nanofluid over riga plate: Numerical analysis. *Energies* **2022**, *15*, 316.
10. Parvine, M.; Alam, M.M. Nanofluid flow along the riga plate with electromagnetic field in a rotating system. *AIP Conf. Proc.* **2019**, *2121*, 070003. [CrossRef]
11. Abbas, T.; Ayub, M.; Bhatti, M.M.; Rashidi, M.M.; Ali, M.E.S. Entropy generation on nanofluidflow through a horizental riga plate. *Entropy* **2016**, *18*, 223. [CrossRef]
12. Sannad, M.; Hussein, A.K.; Abidi, A.; Homod, R.Z.; Biswal, U.; Ali, B.; Kolsi, L.; Younis, O. Numeical study of MHD natural convection inside a cubical cavity loaded with copper-water nanofluid by using a non-homogeneous dynamic mathematical model. *Mathematics* **2022**, *10*, 2072. [CrossRef]
13. Awan, A.U.; Ahammad, N.A.; Majeed, S.; Gamaoun, F.; Ali, B. Significance of hybrid nanoparticles, Lorentz and Coriolis forces on the dynamics of water-based flow. *Int. Commun. Heat Mass Transf.* **2022**, *135*, 106084. [CrossRef]
14. Elanchezhian, E.; Nirmalkumar, R.; Balamurugan, M.; Mohana, K.; Prabu, K.M.; Viloria, A. Heat and mass transmission of an Oldroyd-B nanofluid flow through a stratified medium with swimming of motile gyrotactic microorganisms and nanoparticles. *J. Therm. Anal. Calorim.* **2020**, *141*, 2613–2623. [CrossRef]
15. Loganathan, K.; Mohana, K.; Mohanraj, M.; Sakthivel, P.; Rajan, S. Impact of third-grade nanofluid flow across a convective surface in the presence of inclined Lorentz force: An approach to entropy optimization. *J. Therm. Anal. Calorim.* **2020**, *144*, 1935–1947. [CrossRef]
16. Ahmad, S.; Khan, M.I.; Hayat, T.; Khan, M.I.; Alsaedi, A. Entropy genertion optimization and unsteady squeezing flow of viscous fluid with five different shapes of nanoparticles. *Colloids Surf. A Physicochem. Eng. Asp.* **2018**, *554*, 197–210. [CrossRef]
17. Loganathan, K.; Rajan, S. An entropy approach of Williamson nanofluid flow with Joule heating and zero nanoparticle mass flux. *J. Therm. Anal. Calorim.* **2020**, *141*, 2599–2612. [CrossRef]
18. Waqas, H.; Farooq, U.; Muhammad, T.; Hussain, S.; Khan, I. Thermal effect on bioconvection flow of Sutterby fluid between two rotating diskswith motiole microorganisems. *Case Stud. Therm. Eng.* **2021**, *26*, 101136. [CrossRef]
19. Yahya, A.U.; Salamat, N.; Habib, D.; Ali, B.; Hussain, S.; Abdal, S. Implication of Bio-convection and Cattaneo-Christov heat flux on Williamson Sutterby nanofluid transportation caused by a stretching surface with convective boundary. *Chin. J. Phys.* **2021**, *73*, 706–718. [CrossRef]
20. Fayyadh, M.M.; Naganthran, K.; Basir, M.F.M.; Hashim, I.; Roslan, R. Raiative MHD Sutterby Nanofluid Flow Past a Moving Sheet: Scaling Group Analysis. *Mathemtics* **2020**, *8*, 1430.

21. Gowda, R.J.P.; Kumar, R.N.; Rauf, A.; Prasannakumara, B.C.; Shehzad, S.A. Magnetized flow of sutterby nanofluid through cattneo-christov theory of heat diffusion and stefan blowing condition. *Appl. Nanosci.* **2021**. [CrossRef]
22. Aldabesh, A.; Haredy, A.; Al-Khaled, K.; Khan, S.U.; Tlili, I. Darcy resistance flow of Sutterby nanofluid with microorganisms with applications of nano-biofuel cells. *Sci. Rep.* **2022**, *12*, 7514. [CrossRef] [PubMed]
23. Hayat, T.; Masood, F.; Qayyum, S.; Alsaedi, A. Sutterby fluid flow subject to homogeneous-heterogeneous reactions and nonlinear radiation. *Phys. A Stat. Mech. Appl.* **2019**, *2019*, 123439. [CrossRef]
24. Fujii, T.; Miyatake, O.; Fujii, M.; Tanaka, H.; Murakami, K. Natural convective heat transfer from a vertical isothermal surface to a non- Newtonian Sutterby fluid. *Int. J. Heat Mass Transf.* **1973**, *16*, 2177–2187.
25. Bilal, S.; Sohail, M.; Naz, R.; Malik, M.Y. Dynamical and optimal procedure to analyse the exhibition of physical attribute imparted by Sutterby magneto nano fluid in Darcy medium yield by axially stretched cylindr. *Can. J. Phys.* **2019**, *98*, 1–10. [CrossRef]
26. Khan, M.I.; Waqas, H.; Farooq, U.; Khan, S.U.; Chu, Y.M.; Kadry, S. Assessment of bioconvection in magentized Sutterby nanofluid configured by a rotating disk: A numerical approach. *Mod. Phys. Lett. B* **2021**, *35*, 2150202. [CrossRef]
27. Sohail, M.; Naz, R. Modified heat and mass transmission models in the magnetohydrodynamic flow of Sutterby fluid flow in stretching cylinder. *Phys. A Stat. Mech. Appl.* **2020**, *549*, 124088. [CrossRef]
28. Saif-ur-Rehman; Mir, N.A.; Alqarni, M.S.; Farooq, M.; Malik, M.Y. Analysis of heat generation/absorption in thermally stratified Sutterby fluid flow with Cattaneo-Christov theory. *Microsyst. Technol.* **2019**, *25*, 3365–3373. [CrossRef]
29. Usman; Lin, P.; Ghaffari, A. Heat and mass transfer in a steady flow of Sutterby nanofluid over the surface of a stretching wedge. *Phys. Scr.* **2021**, *96*, 065003. [CrossRef]
30. Ali, F.; Loganathan, K.; Prabu, E.; Eswaramoorthi, S.; Faizan, M.; Zaib, A.; Chaudhary, D.K. Entropy Minimization on Sutterby Nanofluid past a Stretching Surface with Swimming of Gyrotactic Microorganisms and Nanoparticles. *Math. Probl. Eng.* **2021**, 5759671. [CrossRef]
31. Khan, M.I.; Qayyum, S.; Hayat, T. Stratified flow of Sutterby fluid homogeneous-heterogeneous reaction and Cattaneo-Christov heat flux. *Int. J. Numer. Methods Heat Fluid Flow* **2019**, *29*, 2977–2992. [CrossRef]
32. Kuznestov, A.V.; Nield, D.A. Natural convective boundary layer flow of a nanofluid past a verticle plate. *Int. Therm. Sci.* **2010**, *49*, 243–247.
33. Kuznetsov, A.V. The onset of nanofluid bioconvection in a suspension containing both nanoparticles and gyrotactic microorganisms. *Int. Commun. Heat Mass Transf.* **2010**, *37*, 1421–1425. [CrossRef]
34. Kotha, G.; Kolipaula, V.R.; Rao, M.V.S.; Penki, S.; Chamkha, A.J. Internal heat generation on bioconvection of an MHD nanofluid flow due to gyrotactic microorganisms. *Eur. Phys. J. Plus* **2020**, *135*, 135–600. [CrossRef]
35. Siddiq, M.K.; Ashraf, M. Bioconvection of micropolar nanofluid with modified cattaneo-christov theories. *Adv. Mech. Eng.* **2020**, *12*, 1687814020925217. [CrossRef]
36. Bagh, A.; Sajjad, H.; Yufeng, N.; Liaqat, A.; Ul, H.S. Finite element simulation of bioconvection and cattaneo-Christov effects on micropolar based nanofluid flow over a vertically stretching sheet. *Chin. J. Phys.* **2020**, *68*, 654–670.
37. Azam, M.; Mahbood, F.; Khan, M. Bioconvection and activation energy dynamisms on radiative sutterby melting nanomaterial with gyrotactic microorganism. *Case Stud. Therm. Eng.* **2022**, *30*, 101749.
38. Khashi'ie, N.S.; Arifin, N.M.; Pop, I.; Nazar, R. Dual solutions of bioconvection hybrid nanofluid flow due to gyrotactic microorganisms towards a vertical plate. *Chin. J. Phys.* **2021**, *72*, 461–474. [CrossRef]
39. Azam, M. Bioconvection and nonlinear thermal extrusion in development of chemically reactive Sutterbynano-material due to gyrotactic microorganisms. *Int. Commun. Heat Mass Transf.* **2022**, *130*, 105820. [CrossRef]
40. Hayat, T.; Inayatullah, A.; Alsaedi, A. Development of bioconvection flow of nano-material with melting effects. *Chaos Solitons Fractals* **2021**, *148*, 111015. [CrossRef]
41. Reddy, C.S.; Ali, F.; Ahmed, M.F.A.F. Aspect on unsteady for MHD flow of cross nanofluid having gyrotactic motile microorganism due to convectively heated sheet. *Int. J. Ambient Energy* **2021**. [CrossRef]
42. Sarkar, S.; Kumar, T.; Ali, A.; Das, S. Themo-bioconvection of gyrotactic microorganisms in a polymer solution near a perforated Riga plate immersed in a DF medium involving heat radiation, and Arrhenius kinetics. *Chem. Phys. Lett.* **2022**, *797*, 139557. [CrossRef]
43. Ali, F.; Zaib, A. Unsteady flow of an Eyring-Powell nanofluid near stagnation point past a convectively heated stretching sheet. *Arab J. Basic Appl. Sci.* **2019**, *26*, 215–224. [CrossRef]
44. Rana, S.; Nawaz, M. Investigation of enhancement of heat transfer in Sutterby nanofluid using Koo-Kleinstreuer and Li (KKL) correlations and Cattaneo-Christov heat flux model. *Phys. Scr.* **2019**, *94*, 115213. [CrossRef]
45. Mehmood, A.; Ali, A.; Shah, T. Heat transfer analysis of unsteady boundary layer flow by homotopy analysis method. *Commun. Nonlinear Sci. Numer. Simul.* **2008**, *13*, 902–912. [CrossRef]
46. Karthik, T.S.; Loganathan, K.; Shankar, A.N.; Carmichael, M.J.; Mohan, A.; Kaabar, M.K.; Kayikci, S. Zero and nonzero mass flux effects of bioconvective viscoelastic nanofluid over a 3D Riga surface with the swimming of gyrotactic microorganisms. *Adv. Math. Phys.* **2021**, *2021*, 9914134. [CrossRef]
47. Saeed, A.; Kumam, P.; Nasir, S.; Gul, T.; Kumam, W. Non-linear convective flow of the thin film nanofluid over an inclined stretching surface. *Sci. Rep.* **2021**, *11*, 18410. [CrossRef]

48. Loganathan, K.; Sivasankaran, S.; Bhuvaneswari, M.; Rajan, S. Second-order slip, cross-diffusion and chemical reaction effects on magneto-convection of Oldroyd-B liquid using Cattaneo-Christov heat flux with convective heating. *J. Therm. Anal. Calorim.* **2019**, *136*, 401–409. [CrossRef]
49. Eswaramoorthi, S.; Loganathan, K.; Jain, R.; Gyeltshen, S. Darcy-Forchheimer 3D Flow of Glycerin-Based Carbon Nanotubes on a Riga Plate with Nonlinear Thermal Radiation and Cattaneo-Christov Heat Flux. *J. Nanomater.* **2022**, *2022*, 5286921. [CrossRef]
50. Gul, T.; Rehman, M.; Anwar, S.; Khan, I.; Khan, A.; Nasir, S.; Bariq, A. Magnetohydrodynamic impact on Carreau thin film couple stress nanofluid flow over an unsteady stretching sheet. *Math. Probl. Eng.* **2021**, *2021*, 8003805. [CrossRef]
51. Loganathan, K.; Alessa, N.; Kayikci, S. Heat Transfer Analysis of 3-D Viscoelastic Nanofluid Flow Over a Convectively Heated Porous Riga Plate with Cattaneo-Christov Double Flux. *Front. Phys.* **2021**, *9*, 641645. [CrossRef]
52. Wang, C.Y. Free Convection on a Vertical Stretching Surface. *Z. Angew. Math. Mech.* **1989**, *69*, 418–420. [CrossRef]
53. Gorla, R.S.R.; Sidawi, I. Free convection on a vertical stretching surface with suction and blowing. *Appl. Sci. Res.* **1994**, *52*, 247–257. [CrossRef]
54. Khan, W.A.; Pop, I. Boundary-layer flow of a nanofluid past a stretching sheet. *Int. J. Heat Mass Transf.* **2010**, *53*, 2477–2483. [CrossRef]